Computational study of anisotropic epitaxial recrystallization in 4H-SiC

2008 J. Phys.: Condens. Matter 20 125203

(http://iopscience.iop.org/0953-8984/20/12/125203)

J. Phys.: Condens. Matter **20** (2008) 125203 (8pp) doi:10.1088/0953-8984/20/12/125203

Computational study of anisotropic epitaxial recrystallization in 4H-SiC

F Gao[1,3], Y Zhang[1], M Posselt[2] and W J Weber[1]

[1] Pacific Northwest National Laboratory, MS K8-93, PO Box 999, Richland, WA 99352, USA
[2] Forschungszentrum Dresden-Rossendorf, Institute of Ion Beam Physics and Materials Research, PO Box 510119, D-01314 Dresden, Germany

E-mail: fei.gao@pnl.gov

Received 21 November 2007, in final form 25 January 2008
Published 25 February 2008
Online at stacks.iop.org/JPhysCM/20/125203

Abstract

Two nano-sized amorphous layers were created within a crystalline cell to study anisotropic expitaxial recrystallization using molecular dynamics (MD) methods in 4H-SiC. Both amorphous layers were created with the normal of the amorphous–crystalline (a–c) interfaces along the [0001] direction, but one had a microscopic extension along the $[\bar{1}2\bar{1}0]$ direction, i.e. the dimension along the $[\bar{1}2\bar{1}0]$ direction is much larger than that along the $[\bar{1}010]$ direction (I_x model), and the other had a microscopic extension along the $[\bar{1}010]$ direction (I_y model). The amorphous layer within the I_x model can be completely recrystallized at 2000 K within an achievable simulation time, and the recrystallization is driven by a step-regrowth mechanism. On the other hand, the nucleation and growth of secondary ordered phases are observed at high temperatures in the I_y model. The temperature for recrystallization of the amorphous layer into high-quality 4H-SiC is estimated to be below 1500 K. Compared with other models, it is found that the regrowth rates and recrystallization mechanisms depend strongly on the orientation of 4H-SiC, whereas the activation energy spectra for recrystallization processes are independent of any specific polytypic structure, with activation energies ranging from 0.8 to 1.7 eV.

(Some figures in this article are in colour only in the electronic version)

1. Introduction

Because of the unique material properties of silicon carbide (SiC), including a wide band gap, mechanical strength, high thermal conductivity, high melting point and inertness to exposure in harsh environments, SiC represents an attractive semiconductor with a wide range of technological applications, such as optoelectronic devices and high-power, high-temperature electronics [1], as well as structural components in nuclear reactors [2, 3]. Recently, the development and fabrication of high-power electronic devices based on SiC have progressed [4]. For industrial-scale SiC-device fabrication, ion implantation is a major technique for electrical dopant incorporation, since conventional diffusion-based techniques cannot be applied due to the very low diffusivity of dopants [5, 6]. The inescapable presence of defects introduced by the ion implantation of dopants or by neutron irradiation, as well as in wafer growth processes, can significantly degrade the performance of electronic devices and structural components in nuclear applications. In order to achieve comparable electrical conductivity of SiC compared to Si semiconductor, donor or acceptor doping requires ion implantation to high doses, which leads to disorder and amorphization due to the accumulation of damage at room temperature. Thermal annealing at high temperature is generally required to reduce the lattice damage and to electrically activate the implanted species. For instance, solid-phase epitaxial crystallization of ion-beam-amorphized SiC needs temperatures higher than 1723 K [7]. Such extremely high temperatures are not suitable for most device fabrication processes. One way to overcome this problem is to apply ion-beam-induced epitaxial recrystallization, which decreases the critical temperature for recrystallization to about 735 K [8]. However, ion-beam-induced epitaxial recrystallization would lead to the formation of secondary defects and their accumulation can result in poor quality of the recrystallized SiC layer.

Previously, a large number of experimental and theoretical studies have been devoted to understanding amorphous

[3] Author to whom any correspondence should be addressed.

structures, the mechanisms controlling the amorphous-to-crystalline (a–c) transition and the recrystallization process of amorphous SiC. Ivashchenko *et al* [9] employed a tight-binding method to study the atomic and electronic structure of SiC, and found that the topological and local chemical order of the resulting amorphous networks are very sensitive to the initial high-temperature structures. Short- and intermediate-range structural correlations in amorphous SiC were studied using a molecular dynamics method with partial ionic potentials [10], and the atomic mechanisms of the crystalline-to-amorphous transition during nanoindentation were investigated with the same potentials [11]. Furthermore, amorphous-like grains of SiC have been explored to understand deformation mechanisms and to determine the relative stability of nano-sized SiC crystalline particles [12]. An atomic-level model of epitaxial recrystallization in 3C-SiC has been developed to study epitaxial recrystallization, nucleation and growth of secondary ordered phases, and phase transformation in 3C-SiC [13, 14]. The results have shown that the recrystallization mechanism in SiC consists of multiple stages, with initial epitaxial recrystallization of the amorphous layer, which is subsequently hindered by the nucleation of a polycrystalline 2H-SiC phase. Two nano-sized amorphous layers, one with the normal of the a–c interface along the $[\bar{1}2\bar{1}0]$ direction and the other along the $[\bar{1}010]$ direction, were employed to study epitaxial recrystallization and the formation of secondary phases in 4H-SiC [15]. The amorphous layer with the a–c interface normal along the $[\bar{1}2\bar{1}0]$ direction can be completely recrystallized at temperatures of 1500 and 2000 K, while the recrystallization process for the a–c interface normal along the $[\bar{1}010]$ direction at 2000 K is hindered by the nucleation of polycrystalline phases that are stable for much longer simulation times. However, SiC-based devices are predominantly fabricated in epilayers of the 4H-polytype with (0001) faces, because it is easy to achieve a controlled layer-by-layer growth of SiC along this direction.

The recrystallization processes for ion-implantation-induced amorphous layers in 4H-SiC [16, 17] have recently been investigated over the temperature range from 1200 to 1973 K. Satoh *et al* [16, 17] demonstrated that implantation-induced amorphous 4H-SiC epilayers oriented in the $[1\bar{1}00]$ or $[11\bar{2}0]$ direction could largely be recrystallized at 1773 K and preserve the polytype of the underlying layer, whereas [0001]-oriented 4H-SiC epilayers are highly defective and contains various polytype crystals such as 3C-SiC. Furthermore, the regrowth rate for $[11\bar{2}0]$-oriented SiC is faster than that for $[1\bar{1}00]$-oriented samples. These studies provide significant insight into the macroscopic anisotropic recovery of the implantation-induced amorphous layers, but the microscopic mechanisms controlling the recrystallization are far from being established, particularly associated with different atomic stacking along different directions.

In order to understand the dynamic processes of ordering and the pathways to recrystallization, atomic-level simulations are needed to explore the microscopic mechanisms controlling the amorphous-to-crystalline (c–a) transition and epitaxial growth. In the present work, two nano-sized amorphous layers in 4H-SiC, both with a normal of the a–c interfaces along the [0001] direction, were studied. One nano-sized amorphous layer was generated with the lateral dimension along the $[\bar{1}2\bar{1}0]$ direction much larger than that along the $[\bar{1}010]$ direction, and another with the lateral dimension along the $[\bar{1}010]$ direction much larger than that along the $[\bar{1}2\bar{1}0]$ direction. These models represent quasi-two-dimensional SiC, with a one-dimensional a–c interface. A number of features in the epitaxial recrystallization process, including the nucleation and subsequent growth of secondary phases as well as the mechanisms controlling the evolution of these processes, will be reported. The spectrum of activation energies associated with various recrystallization processes will be determined. A comparison of the present results with the previous annealing simulations in $(\bar{1}2\bar{1}0)$- and $(\bar{1}010)$-oriented SiC [13, 15] will be made to address an important issue, i.e. anisotropic epitaxial recrystallization in 4H-SiC.

2. Computational approach

The computational approach in present studies is similar to that employed previously, and thus only the central principles are described. Molecular dynamics (MD) simulations were performed using a modified version of the MOLDY computer code [18]. The interactions between atoms were described by an optimized form of the Brenner-type potential [19] along with the Ziegler–Biersack–Littmark potential [20] for short interatomic separations. The potential form is described in greater detail elsewhere [19], so only the relevant features are summarized here. The potential energy, E, is given as a sum over individual bonds according to the following expression:

$$E = \sum_i \sum_{j(>i)} f_{ij}(r_{ij})[V^{\mathrm{R}}(r_{ij}) - \overline{B}_{ij} V^{\mathrm{A}}(r_{ij})]. \tag{1}$$

The repulsive, V^{R}, and attractive, V^{A}, pair energies are given by the following Morse-type formulation:

$$V^{\mathrm{R}}(r_{ij}) = [D^{\mathrm{d}}/(S-1)] \exp[-\beta\sqrt{2S}(r_{ij} - R^{\mathrm{d}})] \tag{2}$$

and

$$V^{\mathrm{A}}(r_{ij}) = [D^{\mathrm{d}} S/(S-1)] \exp[-\beta\sqrt{2/S}(r_{ij} - R^{\mathrm{d}})], \tag{3}$$

where D^{d} and R^{d} are the dimer bond energy and distance, and β and S are adjustable parameters. The cut-off function, $f_{ij}(r_{ij})$, is defined as:

$$f_{ij}(r) = \begin{cases} 1, & r_{ij} \leqslant R_1 \\ 0.5[1 - \sin\{\pi(r_{ij} - R_1)/(R_2 - R_1)\}], & R_1 < r_{ij} \leqslant R_2 \\ 0, & r_{ij} > R_2, \end{cases} \tag{4}$$

where R_1 and R_2 are adjustable parameters. The many-body interaction is given by:

$$\overline{B}_{ij} = 0.5[B_{ij}^{-\delta_i} + B_{ji}^{-\delta_j}],$$
$$B_{ij} = 1 + \sum_{k \neq i,j} f_{ik}(r_{ik}) g_i(\theta_{ijk}), \tag{5}$$

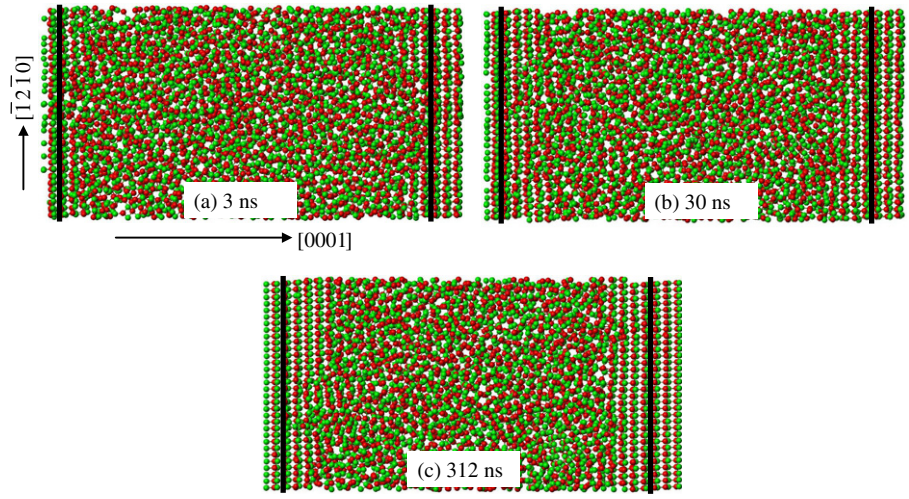

Figure 1. The recrystallization process in model I_x, as defined in the text, as a function of time, where red spheres indicate Si atoms and green spheres represent C atoms. Two solid lines in atomic plots indicate the initial position of the a–c interfaces.

Table 1. Potential parameters for SiC, showing three types of interaction between C–C, Si–C and Si–Si.

Parameter	C	Si	Si–C
R^{d} (Å)	1.515	2.197	1.7631
D^{d} (eV)	4.265	2.887	4.682
β (Å^{-1})	1.50	1.469	1.728
S	1.44	1.32	1.541
δ	0.804 69	0.78	—
R_1 (Å)	2.2	2.2	2.2
R_2 (Å)	2.5	2.5	2.5
α_i	0.011 304	0.013 318	—
c_i	19	14	—
d_i	2.5	2.1	—

where the angular function $g(\theta)$ is given by

$$g_i(\theta_{ijk}) = \alpha_i\{1 + c_i^2/d_i^2 - c_i^2/[d_i^2 + (1 + \cos\theta_{ijk})^2]\}. \quad (6)$$

The potential parameters are listed in table 1. The potential reliability for recrystallization simulations has been discussed in detail elsewhere [15]. Like the different versions of the Tersoff potential, the potential that is employed considers only short-range interactions with a cut-off between the first and the second neighbor shells of an ideal lattice site. Therefore, the current potential predicts the same bulk properties of 4H-SiC as those of 3C-SiC. Since the cohesive energy difference between 4H-SiC and 3C-SiC is very small, it is expected that the potential employed should provide a reasonable approach for simulation studies of recrystallization in SiC.

Two amorphous models were established for the current studies, and they consisted of two-dimensional rectangular simulation cells extended along the [0001] direction, with the amorphous interface normal to the [0001] direction. One nano-sized amorphous layer is generated with the lateral dimension along the [$\bar{1}2\bar{1}0$] direction much larger than that along the [$\bar{1}010$] direction, as shown in figure 1(a) (denoted as an I_x model), and the other with the lateral dimension along the [$\bar{1}010$] direction much larger than that along the [$\bar{1}2\bar{1}0$] direction (I_y model). The simulation cells consisted of $20c_0 \times 16a_0 \times 2\sqrt{3}a_0$ (10 240 atoms) and $20c_0 \times 10\sqrt{3}a_0 \times 3a_0$ (9600 atoms) unit cells for the models I_x and I_y, respectively, where a_0 and c_0 are the lattice constants of 4H-SiC. Periodic boundary conditions were applied to all three directions. The use of periodic boundary conditions in the two lateral directions may lead to certain limitations, since not all regrowth modes can be simulated. However, we have carefully checked this size effect by changing the lateral extensions of the MD box, and noticed that the general regrowth features are very similar to those observed in the present quasi-two-dimensional models of SiC. Generally, most computational models of solid-phase epitaxial regrowth assume that the two lateral extensions of the MD box are equal. However, this is an idealized assumption, since in real systems the lateral extensions are not always equal. In the present work different lateral extensions are considered, and one is larger than the other. Therefore, the present work investigates the two corresponding real systems.

Similar to previous studies [15], the MD block was divided along the longitudinal axis into 40 layers, and each layer contained 256 and 240 atoms in the models I_x and I_y, respectively. A Gaussian-profile heat spike was initiated by applying a suitable distribution of kinetic energy to the atoms of the central 20 layers, with a maximum temperature of 6000 K. The crystal was equilibrated for 0.2 ns to allow full mixing in the central region of the crystal, and then quenched to 0 K at the rate of 10^{13} K s^{-1}. The quenching rate was high compared to the experimental conditions, but the effects of different quenching rates on the amorphous structures were small [15]. The system was relaxed for another 50 ps under zero-external-pressure conditions to eliminate the internal stresses that may develop during the quenching process.

The atomic structure in the central region of the crystal did not exhibit any evidence of long-range order, consistent with an amorphous layer. Two interfaces were created between the amorphous phase and the crystalline host phase. An analysis

of the pair-correlation function, bond angles and bond lengths indicated that the central disordered region is a liquid-like structure that is consistent with an amorphous state. The amorphous structure is similar to those obtained in $(\bar{1}2\bar{1}0)$- and $(\bar{1}010)$-oriented SiC (see the details in figure 1 of [15]). The calculated partial pair-correlation functions demonstrate that the first nearest neighbor is centered at 0.186 nm for Si–C pairs, and the second nearest neighbors are centered at 0.304 and 0.308 nm for Si–Si and C–C pairs, respectively. These peaks correspond to the short-range order in crystalline SiC. However, C–C and Si–Si homonuclear bond peaks are visible at about 0.17 and 0.26 nm, respectively. The bond angles in the amorphous region show a broad distribution ranging from 65° to 160°, indicating that the nature of the bonding has changed from that in perfect SiC. In the amorphous (a-SiC) layer, long-range order does not exist, but partial short-range chemical order is still retained, which can be quantified by the fraction of homonuclear bonds [15, 21]. The short-range disorder parameter for the central region of the crystals was calculated to be 0.15, which is consistent with the value of 0.14 obtained in $(\bar{1}2\bar{1}0)$- and $(\bar{1}010)$-oriented SiC.

To initiate annealing simulations, both models were rescaled to a specific annealing temperature. The annealing simulations were carried out under constant pressure ($p = 0$) and temperature conditions, with simulation annealing times extending to 312 ns. As noted previously [15], the recrystallization processes for the amorphous layer and the disorder-to-order transformations can be described quantitatively using the amorphous fraction, defined as a ratio of amorphous atoms to the total number atoms in the system. Based on the criteria suggested by Marqués *et al* [22], a method has been developed to identify crystalline and amorphous atoms by comparing two sets of calculations at the same temperature. The atomic positions and three-body correlation function for a perfect crystal and a crystal containing an amorphous layer are averaged for a time of about 2 ps to eliminate possible errors due to fluctuation. If a Si or a C atom is fourfold coordinated with its neighbors (C or Si atoms) and the six possible angles between the corresponding bonds fall within the limits of the averaged distribution for a perfect crystal at the same temperature, the atom is considered to be crystalline. Conversely, if this condition is not fulfilled, the atom is denoted as part of an amorphous network. By applying this criterion to the central region of the melting simulation cells, it was found that about 96% of the atoms belong to the amorphous network (these atoms can be defined as effectively amorphous atoms). After quenching and relaxation of the prepared sample, the fraction of amorphous atoms drops to about 80%.

3. Results and discussions

3.1. Annealing simulation of I_x model

In the I_x model, the amorphous layer extends along the [0001] direction with the lateral extension along the $[\bar{1}2\bar{1}0]$ direction. The preliminary results for this configuration as a result of annealing at 2000 K have been reported previously [23], and only epitaxial regrowth of a crystalline state at the interfaces is observed. The recrystallized SiC grows epitaxially from the original amorphous/crystalline interfaces, and the crystalline portion increases with increasing time. Complete recrystallization is achieved in about 65 ns, and the original crystal structure of 4H-SiC is recovered. During the annealing simulations, excess interstitials or defect clusters are observed, and they stimulate the nucleation and growth of planar defects. The final structure consists of some dislocation loops at the center of the simulation cell. These atomic-level structures are similar to those found in $(\bar{1}2\bar{1}0)$-orientated 4H-SiC, and are in good agreement with experimental observations on post-irradiation annealing of damage accumulation in (0001)-orientated 4H-SiC [24]. The effects of implantation temperature and ion flux on damage accumulation on both the Si and C sublattices in (0001)-orientated 4H-SiC were investigated under Al ion irradiation [24], and the amorphous sample layer annealed at a temperature of 450 K. The microstructural features studied by cross-sectional transmission electron microscopy (TEM) revealed that planar defects were formed through the agglomeration of excess Si and C interstitials during post-irradiation annealing, and some vacancy clusters were also observed.

In the present study, the amorphous layer in the I_x model is also annealed at lower temperatures of 1000, 1250 and 1500 K, with simulation times of up to several hundred nanoseconds. Although the amorphous fraction at the center of the amorphous layer decreases with increasing time, complete recrystallization has not been observed within the achievable simulation times. For instance, figure 1 shows three snapshots at different times during the annealing simulations at 1500 K, where the atomic projections are viewed perpendicular to the interfaces on the [0001]/$[\bar{1}2\bar{1}0]$ plane. The solid lines in the plots indicate the original interface positions. These atomic configurations clearly illustrate the movement of the two a–c interfaces with time and the reduction in the number of amorphous atoms, which demonstrates that recrystallization takes place continuously with increasing time. However, even if the simulation time is extended to 312 ns, the nucleation of secondary ordered phases at the interfaces or within the amorphous layer is not observed. These results, together with the complete recrystallization observed at 2000 K, suggest that the recrystallization process in the I_x model is driven by epitaxial regrowth only, in contrast to that in the I_y model (see the details below). It is interesting to note that the amorphous layer in $(\bar{1}2\bar{1}0)$-orientated 4H-SiC (M_x model) can be recrystallized in accordance with the polytypic structure of the original 4H-SiC at 1500 and 2000 K [15], and the recrystallization process involves only epitaxial regrowth. The consistency between these two models implies that the amorphous layer associated with the $[\bar{1}2\bar{1}0]$ direction, either parallel or perpendicular to the a–c interfaces, can be completely recrystallized to the original polytypic structure of 4H-SiC without forming any secondary ordered phases.

However, the growth rate along the $[\bar{1}2\bar{1}0]$ direction in the M_x model is much faster than that along the [0001] direction

in the I_x model. The time for complete recrystallization in the M_x model is, for example, about 12 ns at 2000 K, whereas it is about 65 ns in the I_x model. The slower regrowth rate in the I_x model, compared with the M_x model, may be correlated to the density of atomic planes and the atomic stacking sequences of the interface normal. Figure 2 shows the atomic staking sequences in the $(\bar{1}010)$ plane for (a) $(\bar{1}2\bar{1}0)$-orientated (M_x) and (b) (0001)-orientated 4H-SiC (I_x), where symbols *h* and *c* denote the hexagonal and cubic sites, respectively, as defined in [25]. In the M_x model, the atomic stacking sequence in the a–c interface lies along the [0001] direction, and the hexagonal- and cubic-bond atoms are located at different planes. Also, there exist both hexagonal- and cubic-bond atoms at the interface, and therefore Si and C atoms in the amorphous layer can easily rearrange in accordance with the original polytype structure during regrowth. In the I_x model, the a–c interface is formed perpendicular to the [0001] direction, such that only one type of atoms (hexagonal or cubic) exists at the interface. Complete recrystallization along the (0001) direction involves a two-step process. As shown in figure 2(b), the atomic plane grown from the amorphous layer has to be a C plane, and then the atoms in this plane have to form hexagonal bonds. These restrictions during the recrystallization process may lead to the atomic stacking sequence disappearing at the interface. However, it is observed that the recrystallization occurs parallel to the interface along the $[\bar{1}2\bar{1}0]$ direction, rather than along the [0001] direction in the I_x model, which allows an easier pathway for the amorphous layer to be completely recrystallized. As shown in figure 1, the interfaces are not planar, and have a zigzag character that forms a number of steps along the interfaces. These steps play an important role in the regrowth along the $[\bar{1}2\bar{1}0]$ direction, with behavior that is similar to the recrystallization process in the M_x model. However, the formation of steps and the following regrowth in the I_x model could increase the growth rate compared to the M_x model.

3.2. Annealing simulation of I_y model

In the I_y model, the amorphous layer extends along the [0001] direction with the lateral extension along the $[\bar{1}010]$ direction. Three snapshots of atomic structures annealed at 2000 K are shown in figure 3 for the recrystallized states after 1, 7 and 205 ns. The atomic projections are viewed perpendicular to the interfaces on the $[0001]/[\bar{1}010]$ plane. The epitaxial regrowth of a crystalline state at the interfaces and the movement of the interfaces are generally similar to those observed in the models that extend along the $[\bar{1}2\bar{1}0]$ (denoted as M_x) and $[\bar{1}010]$ (M_y) directions [15], i.e. the recrystallized SiC grows epitaxially from the original a–c interface, and the crystalline fraction increases with increasing time, as shown in figures 3(a) and (b). In addition to the epitaxial recrystallization at the interfaces, it is also observed that secondary ordered phases nucleate and grow at the interfaces and within the amorphous region. The circles in figure 3(b) indicate four distinct nucleation sites, where two of them are near the interfaces and the other two are inside the amorphous region. These nucleation sites serve as seeds for the growth of the secondary ordered phases.

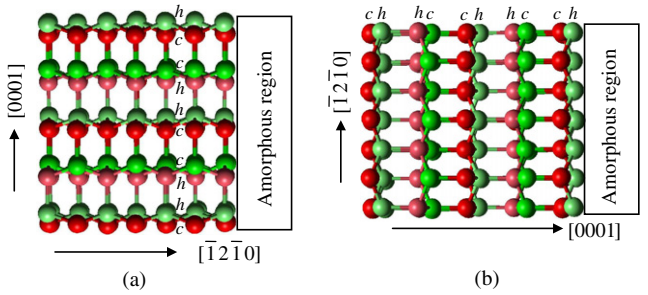

Figure 2. Schematic illustration of atomic arrangement and interfaces in the $(\bar{1}010)$ plane for (a) $(\bar{1}2\bar{1}0)$-orientated 4H-SiC (the model M_x) and (b) (0001)-orientated 4H-SiC with the a–c interface along the $[\bar{1}2\bar{1}0]$ direction (the model I_x), where atom representation is the same as in figure 1. Symbols h and c denote the hexagonal and cubic bonds, respectively.

Two nucleation sites, as indicated by the blue circles, grow into 4H-SiC with the same crystallographic orientations as those of the original crystal, but the other two form polytype microcrystalline domains that are indicated by the dashed lines in figure 3(c). These microcrystals form a continuous network embedded in the perfect 4H-SiC, and the formation of the secondary ordered phases at the interfaces hinders the epitaxial recrystallization process in 4H-SiC. Complete recrystallization is achieved after about 36 ns (not shown in figure 3) at 2000 K, and the final structure of the recrystallized state is shown in figure 3(c). The atoms at the grain boundaries are partially disordered, and the transition regions between different grains consist of a few atomic layers. However, there exists a number of dangling bonds at the grain boundaries, and segregation of interstitial defects is observable at the grain boundaries. Although the structures of the grain boundaries change slightly during further annealing, these structures are very stable, which may suggest that higher temperatures and longer simulations may be required to completely recover the 4H structure. These results are generally similar to those observed in the recrystallization model with the a–c interface normal along the $[\bar{1}010]$ direction [15], i.e. the recrystallization is hindered by the nucleation of polycrystalline phases at 2000 K, and these secondary phases are stable for long simulation times. As described previously [15], different SiC polytypes can be characterized using dimer rows that are perpendicular to the basal plane, and the lattice can be established by a two-dimensional periodic arrangement of the intersections of these dimer rows with the basal plane. There is only one type of dimer row in 3C-SiC, while there are two different rows that lead to two nonequivalent sites for both Si and C in 4H-SiC. By applying this method, the microcrystals in figure 3(c) can be identified as 3C-SiC structures, but with different crystallographic orientations to each other.

The recrystallization process of ion-implantation-induced amorphous layers in 4H-SiC has been investigated experimentally for (0001)-orientated 4H-SiC [16], such that a full comparison can be made. Annealing of the amorphous layers in (0001)-orientated 4H-SiC at 1723 K showed that the regrowth induced other polytype crystals that can be identified as 3C- and 4H-SiC, but their crystallographic orientations were different from those of the original 4H-SiC. The present results

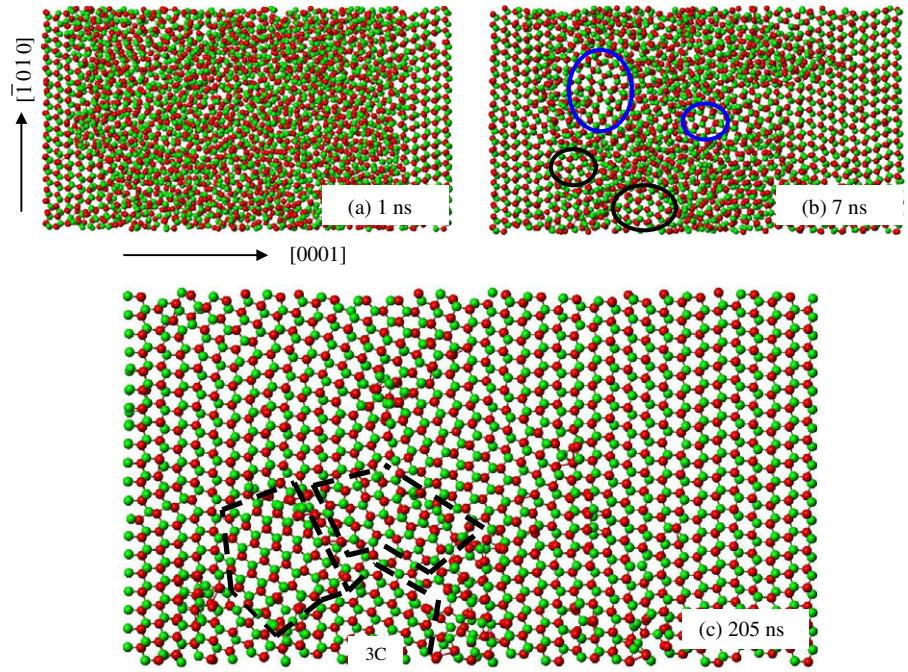

Figure 3. The recrystallization process in the model I_y as a function of time, where atom representation is the same as in figure 1. The nucleation of the secondary ordered phases at the interfaces and inside the amorphous region are indicated by the circles in (b), and the final secondary ordered phases are emphasized by the dashed lines in (c).

are generally consistent with the experimental observations. The nucleation of secondary ordered phases within the amorphous region supports the previous assumption that the formation of these polytype crystals may arise from the random arrangement of Si and C atoms during the regrowth [16]. The present results, along with those of the ($\bar{1}$010)-orientated 4H-SiC model [15], demonstrate that the recrystallization of the amorphous layers extended along the [0001] or [$\bar{1}$010] directions can lead to the formation of secondary phases at 2000 K. However, it is interesting to note that secondary ordered phases can nucleate and grow into large microcrystalline domains at 1500 K in the present model, but only epitaxial recrystallization at the interfaces occurs at the same temperature in the ($\bar{1}$010)-orientated 4H-SiC model [15]. This is consistent with the experimental recrystallization of the amorphous layer in ($\bar{1}$010)-orientated 4H-SiC, in which the amorphous layer recrystallizes with the original polytype structure of 4H-SiC at 1723 K. The present atomic-level simulations clearly indicate that the nucleation of secondary ordered phases depends on the annealing temperature and crystal orientation. The careful control of the annealing temperature in ($\bar{1}$010)-orientated 4H-SiC would allow amorphous layers to recrystallize into high-quality 4H-SiC, and the corresponding temperature without the inclusion of these secondary ordered phases is estimated to be around 1500 K.

3.3. Amorphous fraction and energy spectrum

Using the method described above, the number of perfect and amorphous atoms can be calculated as a function of time in the simulation cells, and then the amorphous fraction can be evaluated. At each annealing simulation temperature, the variation of the amorphous fraction is determined as a function of time. The results for the model I_x are shown in figure 4(a). Similar to the observations in other models [13], the recrystallization progresses through several distinct recrystallization stages as time advances. The initial recovery leads to a rapid decrease in the amorphous fraction within the first few nanoseconds, particularly at high temperatures where the decrease in amorphous fraction is much faster than that at lower temperatures. The initial recovery stage is associated with the annihilation or relaxation of point and bond-type defects at the interfaces, and is followed by one or more additional distinct recrystallization stages. However, the amorphous fraction saturates after these recovery stages at 1000–1500 K. Further annealing was carried out for much longer times (up to 315 ns), but no significant additional recrystallization is observed beyond 60 ns. Based on a recrystallization model developed previously [13], the amorphous fraction can be used to determine the activation energy spectrum for recrystallization. The general approach is based on annealing theory for a distribution of quasi-continuous independent processes that are characterized by a distribution of jump frequencies and activation energies [13]. For a single annealing process with a distribution of activation energies or jump frequencies, the activation energy distribution should exhibit a broad peak, while a process with a specific activation energy and jump frequency should exhibit a sharp peak in the distribution at the characteristic activation energy for that process [13]. By applying this method of analysis to the data in figure 4(a), the activation energy spectra can be determined for each annealing curve. The results are shown in figure 4(b) for recrystallization processes at different temperatures for the I_x model. The overlap of peaks

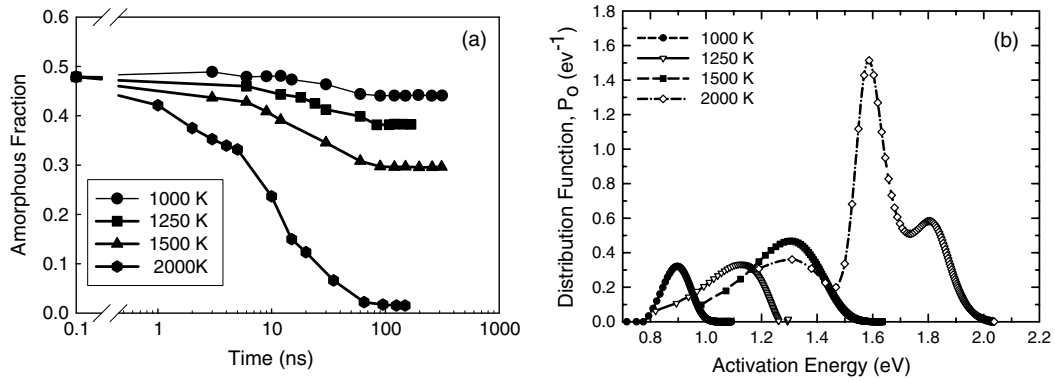

Figure 4. (a) Variation of amorphous fractions as a function of simulation time at different temperatures and (b) activation energy spectra calculated from a model developed previously for recrystallization processes in the model I_x, where the time at each annealing temperature samples different regions of activation energy (time–temperature) space.

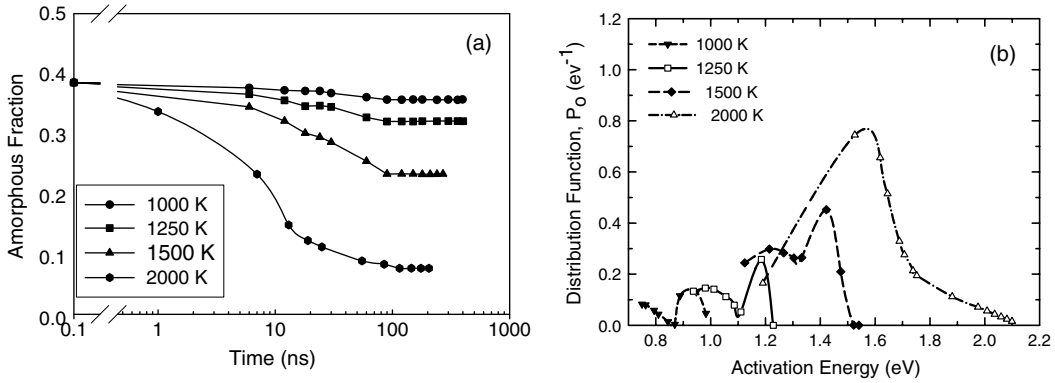

Figure 5. (a) Variation of amorphous fractions as a function of simulation time at different temperatures and (b) activation energy spectra calculated from a model developed previously for recrystallization processes in the model I_y.

in the activation energy spectra yields a nearly continuous spectrum of activation energies for the various recrystallization processes. The first resolved peaks in the activation energy spectra are at about 0.9 and 1.1 eV, and similar energy peaks were previously observed in the studies of epitaxial recrystallization in 3C-SiC [13], and $(\bar{1}2\bar{1}0)$- and $(\bar{1}010)$-orientated 4H-SiC [15] at the same annealing temperatures, and are independent of any specific polytype structure. This confirms that the proposed mechanisms for recovery at low temperatures are associated with the recombination of some close-pairs [26] and for C interstitial migration in SiC [27]. At 1500 K, an activation energy peak is also observed at about 1.3 eV, which is correlated to the initial epitaxial regrowth and atomic arrangement along the $[\bar{1}2\bar{1}0]$ direction, and the cumulative effects of defect relaxation. The rapid recrystallization processes for activation energies below 1.4 eV at 2000 K (as seen in figure 4(a)) are not resolvable on the timescales employed at the temperature. The major recrystallization process at 2000 K for times longer than a few nanoseconds has a unique activation energy peak at about 1.6 eV, as shown in figure 4(b), and this energy represents a full energy peak for epitaxial recrystallization. It can be seen that there is also a small peak at about 1.8 eV that may be associated with the nucleation and formation of dislocation loops, as discussed above.

Figure 5(a) shows the variation in the amorphous fraction as a function of simulation time in the I_y model. The decrease in amorphous fraction with increasing time is very similar to that in the I_x model, and all the data show a rapid decrease in the initial few nanoseconds, followed by several distinct recrystallization stages. However, it can be seen clearly that the reduction in the amorphous fraction becomes slow, typically after 7 ns, at 2000 K, which lasts for about 100 ns. This may be associated with the nucleation of the secondary ordered phases and their growth, which impedes the epitaxial regrowth of the a–c interfaces, and thus slows down the regrowth process. Similar behavior has also been observed for the annealing simulations at 1500 K, which contrasts with the M_y model, where only epitaxial recrystallization at the interfaces occurs. The reduction in the rate of amorphous fraction in the I_y model is similar to that in the I_x model, but much slower than that in the M_y model. For instance, the time for saturation of the amorphous fraction is about 30 ns at 1500 K in the M_y model, but it requires 100 ns in the I_y model. These results clearly demonstrate that the growth rate for the models with a normal to the [0001] direction is slower than that for $(\bar{1}2\bar{1}0)$- and $(\bar{1}010)$-orientated 4H-SiC. As described above, the amorphous fraction can be used to determine the activation energy spectrum for recrystallization by applying the recrystallization model, and the corresponding

results are shown in figure 5(b). The general features of the activation energy spectrum are very similar to those in figure 4(b), i.e. the energy peaks are overlapping, forming an almost continuous spectrum, which is associated with various recrystallization processes, and the activation energy values range from 0.9 to 1.6 eV. All these results demonstrate well that the recrystallization mechanism consists of multiple stages and thus multiple activation energies, which is independent of a specific model or crystallographic orientation. However, it should be noted that the initial amorphous fraction is different for the I_x and I_y models, and the different size of amorphous regions may affect the nucleation of secondary ordered phases. Consequently, much larger MD cells have been used with a simulation time of a few nanoseconds at 2000 K, and the results show that the nucleation of secondary ordered phases has not been observed in the I_x model, but that it does occur in the I_y model. These simulations demonstrate that the size of the amorphous regions is large enough to eliminate possible size effects on the nucleation and growth of secondary ordered phases.

4. Summary

MD methods have been applied to study the anisotropic expitaxial recrystallization of the a–c interfaces in two models of 4H-SiC (I_x and I_y models) at temperatures ranging from 1000 to 2000 K. The amorphous layer within the I_x model can be completely recrystallized at temperature of 2000 K, but the recrystallized region contains interstitial dislocation loops, which is consistent with the experimental observations. The formation of the steps along the direction parallel to the interfaces provides an easy pathway for the amorphous layer to be completely recrystallized. It should be noted that the amorphous layers in the models with either the interface normal or parallel to the $[\bar{1}2\bar{1}0]$ direction can be completely recrystallized to the original polytype structure of 4H-SiC. In the I_y model, the recrystallization process is hindered by the nucleation and growth of the secondary ordered phases that have been identified as 4H- and 3C-SiC with different crystallographic orientations to the original 4H-SiC. This phenomenon is observed only at high temperatures, and the consistency of the present simulations with the previous observations in the M_y model suggests that the temperature for recrystallization of the amorphous layer into high-quality 4H-SiC should be below 1500 K. Also, it is found that the regrowth rate in the (0001)-orientated 4H-SiC (both I_x and I_y models) is much slower than that in $(\bar{1}2\bar{1}0)$- and $(\bar{1}010)$-orientated models.

The activation energy spectra for recrystallization in the I_x and I_y models have been determined, and the results show that there is a number of activation energy peaks associated with different recrystallization processes. Although the recrystallization mechanisms are correlated with the orientations of different 4H-SiC models, the activation energy spectra depend weakly on a specific polytype structure. The activation energies for full recrystallization in 4H-SiC range from 0.8 to 1.7 eV.

Acknowledgments

This research is supported by the Division of Materials Sciences and Engineering, Office of Basic Energy Sciences, US Department of Energy under contract DE-AC05-76RL01830.

References

[1] Bolse W 1999 *Nucl. Instrum. Methods Phys. Res.* B **148** 83
[2] Minato K, Sawa K, Koya K, Tomita T, Ishikawa A, Baldwin C A, Gabbard W A and Malone C M 2000 *Nucl. Technol.* **131** 36
[3] Lake J A, Bennett R G and Kotek J F 2002 *Sci. Am.* **286** 73
[4] Chow T P 2000 Progress in SiC high-voltage power switching devices *UPD2000: 1st Int. Workshop on Ultra-Low-Loss Power Device Technology (Nara, May–June)*
[5] Davies R F, Kelner G, Shur M, Palmour J W and Edmond J A 1991 *Proc. IEEE* **79** 677
[6] Hallén A, Janson M S, Kuznetsov A Yu, Åberg D, Linnarsson M K, Svensson B G, Persson P O, Carlsson F H C, Storasta L, Bergman J P, Sridhara S G and Zhang Y 2002 *Nucl. Instrum. Methods* B **186** 186
[7] Bohn H G, Williams J M, Mchargue C J and Begun G M 1987 *J. Mater. Res.* **2** 107
[8] Heera V, Stoemenos J, Kögler R and Skorupa W 1995 *J. Appl. Phys.* **77** 2999
[9] Ivashchenko V I, Turchi P E A, Shevchenko V I, Ivashchenko L A and Rusakov G V 2002 *Phys. Rev.* B **66** 195201
[10] Rino J P, Ebbsj I, Branicio P S, Kalia R K and Nakano A 2004 *Phys. Rev.* B **70** 045207
[11] Szlufarska I, Kalia R K, Nakona A and Vashishta P 2005 *Phys. Rev.* B **71** 174113
[12] Szlufarska I, Nakano A and Vashishta P 2005 *Science* **309** 911
[13] Gao F, Devanathan R, Zhang Y, Posselt M and Weber W J 2006 *J. Mater. Res.* **21** 1420
[14] Gao F, Devanathan R, Zhang Y and Weber W J 2005 *Nucl. Instrum. Methods* B **228** 282
[15] Gao F, Zhang Y, Posselt M and Weber W J 2006 *Phys. Rev.* B **74** 104108
[16] Satoh M, Okamoto K, Nakaike Y, Kuriyama K, Kanaya M and Ohtani N 1999 *Nucl. Instrum. Methods* B **148** 567
[17] Satoh M, Hitomi T and Suzuki T 2006 *Nucl. Instrum. Methods* B **242** 627
[18] Finnis M W 1988 A molecular dynamics program for simulation of pure metals *UKAEA Report, No. AERER 13182*
[19] Gao F and Weber W J 2002 *Nucl. Instrum. Methods* B **191** 504
[20] Ziegler J F, Biersack J P and Littmark U 1985 *The Stopping and Range of Ions in Matter* (New York: Pergamon)
[21] Yuan Y and Hobbs L W 2002 *Nucl. Instrum. Methods Phys. Res.* B **191** 74
[22] Marqués L A, Caturla M J, Diaz de la Rubia T and Gilmer G H 1996 *J. Appl. Phys.* **80** 6160
[23] Gao F, Zhang Y, Devanathan R, Posselt M and Weber W J 2007 *Nucl. Instrum. Methods* B **255** 136
[24] Zhang Y, Weber W J, Jiang W, Wang C M, Hallén A and Possnert G 2003 *J. Appl. Phys.* **93** 1954
[25] Pirouz P and Yang W J 1992 *Ultramicroscopy* **51** 189
[26] Gao F and Weber W J 2003 *J. Appl. Phys.* **94** 4348
[27] Gao F, Weber W J, Posselt M and Belko V 2004 *Phys. Rev.* B **69** 245205